Scientific Justification

1. Uniqueness of the NEP Survey

The North Ecliptic Pole (NEP) is one of the most frequently visited areas on the sky because of easy accessibility to the space missions. We now have extensive data sets covering almost all wavelengths from UV to radio for a region centered at the NEP, however with some missing bands conspicuous by their absence. In addition, eROSITA, to be launched early 2018, is expected to conduct ultra deep 2-10 keV imaging toward NEP, and we expect unprecedentedly numerous Compton-thick AGNcandidates when combined with the multi-wavelength data in NEP-Wide. We propose to observe the entire NEP-Wide area of ~ 4 sq. deg. with SCUBA-2 850μm to fill the gap between the Herschel 500μm and ground-based radio data at 21cm. By adding the new data from our survey, we will be able to answer the following outstanding questions regarding the evolution of the galaxies:

- What is the origin of the Cosmic Infrared Background? Is it due to the very first population of stars, the intracluster halo stars or something else?
- What is the nature of very red objects and the history of dust obscured star formation?
- What is the role of the AGN in the evolution of galaxies? Under what circumstances do they inhibit or promote star formation?

2. Complete Mid-Infrared Wavelengths Coverage

AKARI, an infrared space telescope developed by Japan in collaboration with international partners including a European Consortium and Korea, made wide area surveys near the NEP. The AKARI NEP survey was carried out in nine infrared wavelength bands between 2 and 24μm. The NEP survey is composed of two parts: NEP-Wide covering about 5.4 sq. degrees and a 0.6 sq. degree area of NEP-Deep to better sensitivity (Matsuhara et al. 2006, see Fig. 1 for the survey regions). The source catalogues have been published for NEP-Deep (Wada et al. 2008, Takagi et al. 2012) and for NEP-Wide (Kim et al. 2012). Ancillary data at various wavelengths have also been obtained at UV-optical (Hwang et al. 2007, Jeon et al. 2010), ground-based near-IR (Jeon et al. 2014), and Radio (White et al. 2010) wavelengths. Spectroscopic observations were carried out for selected sources over the entire NEP-Wide field with MMT/Hectospec and WYIN/HYDRA (Shim et al. 2013). Herschel also observed the NEP-Deep with PACS at 100 and 160μm and the entire NEP-Wide with SPIRE at 250, 350 and 500μm. The NEP is also a candidate deep field for the Euclid mission and is a key target area for the studies of cosmic near infrared background using CIBER, the sounding rocket experiments to detect the near infrared background carried out via imaging and low resolution spectroscopic observations in near infrared (Zemcov et al. 2013). MIRIS, a small Korean Mission in the near infrared just completed a survey of 100 sq. degree centered on NEP with two narrow-band filters, I and H bands (Han et al., 2014). Thus, NEP is one of the most extensively observed areas in the sky in terms of the spectral coverage, while at the same time covering a sufficiently large area to counter the known issues of cosmic variance.

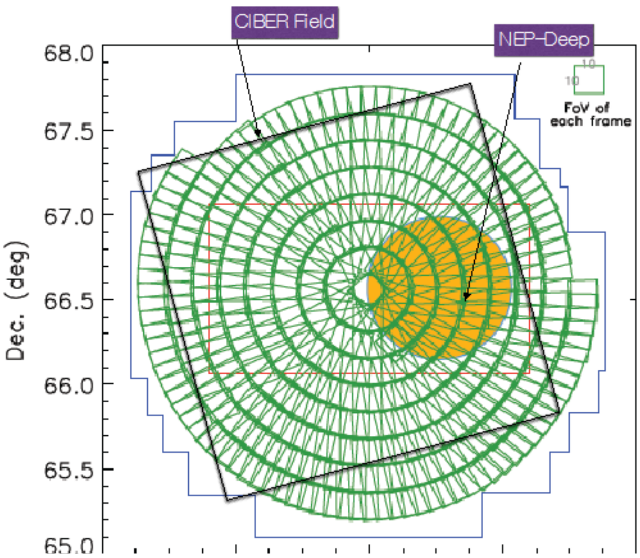

Figure 1. The NEP area with various survey boundaries. Green boxes are individual exposures of the NEP-Wide survey with AKARI. The red rectangle shows the CFHT optical survey area while large black box indicates the CIBER field for the near-infrared background study. The yellow circle is the NEP-Deep area which was one of the SCUBA-2/CLS survey regions.

Current existing datasets over the NEP provide the complete UV-to-MIR spectral energy distributions (SEDs) of low-redshift galaxies within a large range of total infrared luminosity. The key unique point of the NEP data is that it has complete spectral coverage at mid-infrared wavelengths from 2-24μm. Most likely to provide a diversity of PAH emission variation at z < 1, these can also be used to provide information on 3.3μm PAH emission even at z ~ 6. In addition, the 9.7μm and 8μm silicate absorption features, often observed in the spectra of AGN, can provide potent tools for identifying different emission components in the galaxies SEDs. We summarize the existing data over the NEP region in Table 1.

Table 1. Available data for NEP area

Instrument	Bands	Area	Depth (5-σ)	Number of Detected Sources	Reference
GALEX	*FUV/NUV*	~1 sq. deg.	26.1/26.7 AB		Malkan et al. in prep.
CFHT	*u, g, r, i ,z*	~2 sq. deg.	~24 AB	~110,000	Hwang et al. 2007
Maidanak/SNUCAM	*B, R, I*	~4 sq. deg.	22.3-23.5 AB	~100,000	Jeon et al. 2010
KPNO 2.1m /FLAMINGOS	*J, H*	~5.2 sq. deg.	21.4 AB	~220,000	Jeon et al. 2014
AKARI /IRC	2, 3, 4μm 7, 9, 11μm 15, 18μm 24μm	~5.4 sq. deg.	20.9-21.1 AB 19.5-19.0 AB 18.6, 18.7 AB 18.0 AB	~109,000 ~20,000 ~16,000 ~4,000	Kim et al. 2012
MMT/Hectospec & WIYN/HYDRA	Optical (spectroscopy)	~5 sq. deg.	R < 21.5 mag	1645 (spectra)	Shim et al. 2013
WSRT	20cm	~1.7 sq. deg.	0.1 mJy	462	White et al. 2010
Herschel/SPIRE	250, 350, 500 μm	~6 sq. deg.	37.5 – 54 mJy	~3300	Pearson et al. in prep.
Herschel/PACS	100, 160μm	~1 sq. deg.	~20 – 50 mJy	~2400	Pearson et al. in prep.
CIBER	J & H	~4 sq. deg.			Zemcov et al. 2013, 2014
GMRT	610MHz	~2 sq. deg.	~18 uJy	~1630	White et al. in prep.
LOFAR	60-150MHz	~10 sq. deg	~100 uJy	~1800	White et al. in prep.

2. Deep X-ray data will become available with eROSITA

The NEP-Wide is expected to lie entirely within the deepest eROSITA region. The expected 5σ flux limits are 2.9×10^{-14} erg/s/cm^2 for hard (2-10keV) band, and 2.0×10^{-15} erg/s/cm^2 for soft (0.5-2 keV) band (Merloni et al., "eROSITA Science Book"). Thanks to the wide size of NEP-Wide survey, we expect to find ~310 AGNs in this region. An overall picture of the cosmic history of star formation (SFH) as well as the black hole accretion (BHAH) has been revealed now. However, there is a critically big uncertainty in the amount of obscured AGNs and its relation to the SFH and BHAH. In order to solve this, statistically meaningful number of obscured AGNs previously unknown out to z~2 is needed. Here, the new X-ray all-sky surveyor, eROSITA will, when combined with our NEP-Wide infrared (from UV to radio) data, give us such fruitful outcome.

3. The Need for SCUBA-2 850μm Data

The addition of the 850μm SCUBA-2 data to the comprehensive multi-wavelength data over the NEP region will dramatically reduce the uncertainties in SED fitting for infrared sources. The uncertainty of the infrared SED is mainly due to the dust temperature and the dust composition, and such uncertainty propagates to the uncertainties in the derived physical parameters including total infrared luminosity, dust attenuation, star formation rates, and accurate AGN vs. star formation decomposition. Long wavelengths data in the Rayleigh-Jeans side of the infrared SED peak are crucial for reliable infrared SED fitting. Fig. 2 shows the ensemble SEDs of the z < 1 galaxies, which ranges from red, passive galaxies to violently star-forming galaxies. The complete mid-infrared coverage of AKARI/IRC provides a profound opportunity to characterize PAH for galaxies at z < 1, by filling the previous gap of Spitzer between 8-24μm. However, without a data point that reflects cold dust emission at the longer submilimeter wavelengths, it is impossible to construct a full-wavelength model for dusty galaxies and the resulting parameters such as star formation rates, total infrared luminosity, dust attenuation, dust mass, and dust temperatures are highly uncertain.

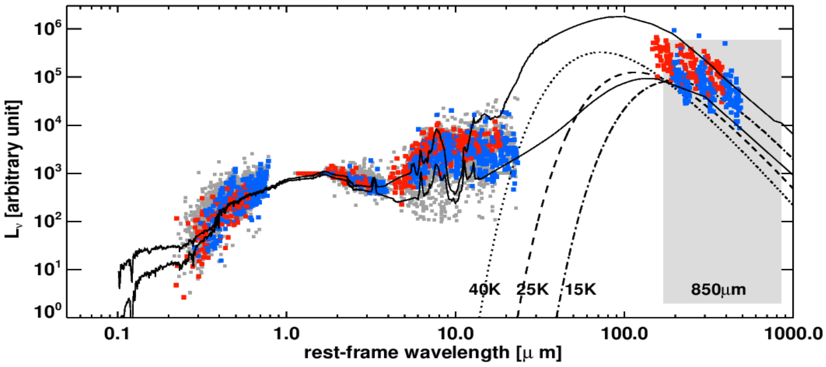

Figure 2. Ensemble SEDs of the galaxies with spectroscopic redshifts of z < 0.3 (blue) and 0.3 < z < 0.8 (red) that are detected in Herschel/SPIRE 250μm band. Gray points are SEDs of the galaxies without 250μm detection at z < 0.8. Dotted, dashed, and dot-dashed line shows how the 850μm data point (covers rest-frame wavelength range for gray shaded region) in addition to Herschel/SPIRE photometry can constrain the dust temperature in these galaxies. Overplotted solid lines are empirical templates of Arp 220 and Sd galaxies (Polletta et al. 2007).

As well as setting constraints on the shape of the IR SED for z < 1 infrared luminous galaxies, sub-millimeter wavelength data also provides the most sensitive tool to observe dusty starbursts at z > 2. This is because of the large negative K-correction at these wavelengths. For example, Fig. 3 shows the expected flux density of the ultra-luminous infrared galaxies with $L_{IR} = 10^{13} L_{sun}$. At 850 μm, the expected flux density remains constant from z ~ 1 to even z ~ 8, while at mid-infrared or shorter wavelengths, the flux density strongly decreases with the redshift. As we already have Herschel/SPIRE 500μm over the NEP, we would be able to directly compare the properties of z ~ 2 galaxies with $L_{IR} = 10^{13} L_{sun}$ and z > 4 galaxies with the same total infrared luminosity, and answer the question whether there exists any evolution in the dust properties and star formation efficiencies as a function of redshift.

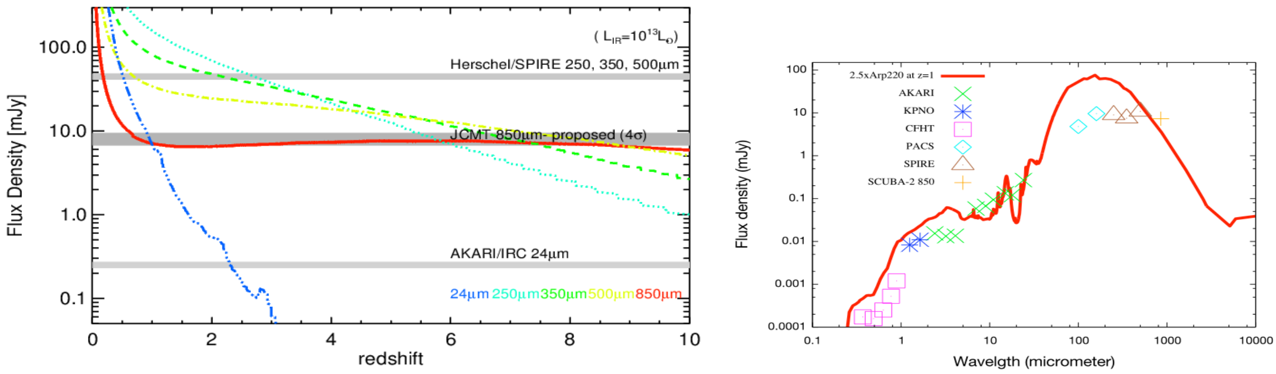

Figure 3. (Left) 4σ flux density limits of infrared-luminous galaxies with $L_{IR} = 10^{13} L_{sun}$ (Pope & Chary 2010) in different infrared filters as a function of redshift. Horizontal lines indicate, from bottom to top, AKARI/IRC 24μm, the proposed SCUBA-2 850μm, and Herschel/SPIRE 3σ flux limits. By adding 850μm data, we would be able to detect 1 < z < 8 extremely infrared-luminous galaxies whose luminosities are comparable to that of the z < 2 infrared-luminous galaxies selected using the existing SPIRE data. Note that these are 4σ flux limits. Therefore in principal it is possible to investigate a few times $10^{12} L_{sun}$ galaxies that are analogous to the local ULIRGs. (Right) Detection limits of the existing surveys toward the NEP region. The Herschel/PACS observation was done only for NEP-Deep region. Also plotted is the SED of Arp 220 galaxy located at the redshift *z*=1. The 4-σ detection limit of the proposed SCUBA-2 survey is also shown with the '+' sign.

Key Science

1. Resolving the Extragalactic Background Light in the Infrared

AKARI IRC data over NEP field have been proved to be useful in detecting cosmic infrared background (CIB: Matsumoto et al. 2011; Zemcov et al. 2013, 2014; Seo et al. 2015). Previous works have shown that there exists excess fluctuation with blue spectrum feature at both small and large angular scale (See Fig. 4). Spatial fluctuations in CIB could either originate from the primordial galaxies and black holes that are reionization populations (e.g., Matsumoto et al. 2011, Kashlinsky et al. 2012; Yue et al. 2013), or from intra-halo scattered light from intra-halo light (IHL) at $z < 1$ (e.g., Cooray et al. 2012; Zemcov et al. 2014). Although recent deep near-infrared observations have preferred the idea of the fluctuation mainly arising from the diffuse IHL not from the reionization population (e.g., Cooray et al. 2012; Zeomcov et al. 2014), there still remains a conflict in interpretation of the observed fluctuation due to the two significant points. First, the cosmic infrared background (CIB) has two peaks, one at near-infrared wavelengths around ~1μm and the other at far-infrared wavelengths around ~250μm (see compilation by Dole et al. 2006). Therefore the interpretation of the observed fluctuation in near-infrared background should also satisfy the interpretation of the observed anisotropy in the far-infrared background. Second, the contribution of low luminosity galaxies at relatively low redshifts that have flux densities below the point source detection level in near- and far-infrared images is not clearly understood, while these galaxies are not masked completely during the fluctuation measurements.

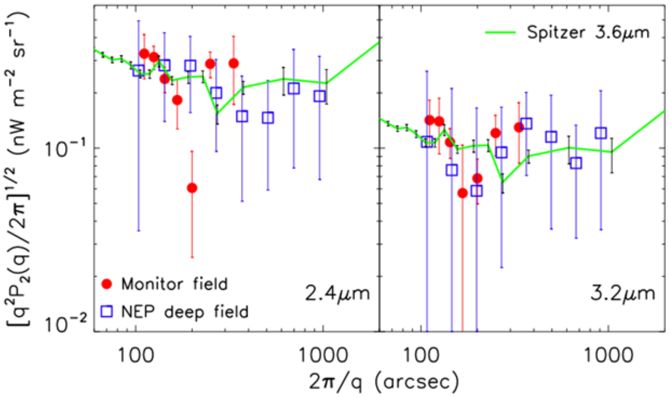

Figure 4. Excess fluctuation of the AKARI Monitor field (filled circles) and the NEP deep field (open squares) (Seo et al. 2015). The green line shows the fluctuation measured with Spitzer data at 3.6μm.

The NEP region is the best region to resolve the above issues thanks to the (1) the intensive coincident near-infrared data useful for detecting cosmic near-infrared background at various angular scales, and (2) the wealth of multi-wavelength data that enables good characterization of the foreground populations. The NEP is the ONLY region visited by both the second and the third flights of the CIBER experiment (see Fig. 1; Zemcov et al. 2014) for the measurement of anisotropies and fluctuation of the cosmic near-infrared background at 1.1μm and 1.6μm. At larger angular scale, the 10° × 10° region centered at the NEP is planned to be observed by MIRIS (Han et al. 2014) though at a shallower depth, which will provide details on fluctuation at angles up to few degrees. Combining the fluctuation at these wavelengths with the measurement by AKARI at 2.4μm and 3.2μm, we would obtain a complete census of the populations that contribute to the near-infrared background. If the far-infrared background fluctuation analysis is combined with these near-infrared studies, we would be able to measure the relative contribution from the possible sources of CIB fluctuation. Thacker et al. (2014) have presented a cross-correlation study of near- and far-infrared background anisotropies using Spitzer 3.6μm and Herschel 250, 350, and 500μm data, separating the contribution of each of the components such as far-infrared faint galaxies under the point source sensitivity, near-infrared faint galaxies under the point source sensitivity, and diffuse intra-halo light. Since the cross-correlation signal decreases as the far-infrared wavelengths increases from 250 to 500μm, they have concluded that most of the CIB is from the IHL.

However, using ~500μm far-infrared data is not sensitive enough to detect the cross-correlation signal from the $z > 6$ populations that are actually responsible for reionization, as we can see in Fig. 3. Instead, the proposed SCUBA-2 850μm data would play a crucial role to detect signals from high-redshift, dusty galaxies and their contribution to the observed CIB anisotropies. Matching the pixel scales of the observed images, pixel by pixel SED fitting using the 850μm excess positions to correlate with the near-infrared background would enable us to calculate the cross-correlation function. This analysis is only possible with the wealth of multi-wavelength data over the NEP region. As we have complete coverage from UV to mid-infrared wavelengths for photometric data points, and spectroscopic redshifts that will increase the reliability of the photometric redshifts for mid-infrared sources, we can better characterize the low-redshift, i.e., foreground objects, therefore providing a direct test for the CIB fluctuation models.

2. Dust Enrichment and Obscured Star Formation in Low- and High-redshift Galaxies

2-1 Red Objects

The 850 μm data in the 'Rayleigh-Jeans' side of the infrared SED peak will help us to better fit the SEDs of dusty galaxies so that we can obtain robust measurements of dust properties such as temperature and mass as well as obscured star formation rates. Quantifying the dust properties is important because the combination of dust and stellar properties provides constraints on the possible evolutionary connection among dusty galaxies at different epochs. Numerous dusty populations such as dust obscured galaxies (DOGs) and sub-millimeter galaxies (SMGs) have been discovered. Recently, it is also known that red, massive distant populations such as distant red galaxies (DRGs) and extremely red objects (EROs) can be split into old and dusty populations. These objects are regarded as progenitors of local massive elliptical galaxies. However, it is still necessary to investigate each population to understand the evolutionary path and the formation of massive galaxies in the local universe.

Fig. 5 shows a SCUBA-2 850μm Daisy map with rms of 1.5mJy over CFHTLS-W2 region (PI: J.-W. Kim, M15AI027). The brightest source (circle) has a flux density of ~10mJy, similar to sources that will be detectable with the proposed SCUBA-2 survey of the NEP field. The inset shows the SED fit of this object to the multi-wavelength data. Colors of this object satisfy color criteria for both EROs and DRGs, which are $(i\text{-}K)_{AB} > 2.45$ for EROs and $(J\text{-}K)_{AB} > 1.3$ for DRGs. In the central 2 sq. degree region of the proposed field with deep i-band images from CFHT, we have found ~1000 EROs. Among these, 50-60 are also detected at both 18μm and 24μm, which implies that these are bright dusty galaxies. We also note that 3-4 EROs were detected with >8mJy in ~100 sq. arcmin area from the previous studies with SCUBA (Smail et al. 1999; Clements et al. 2004; Webb et al. 2004). In addition to EROs, there are several hundreds of DRGs and star-forming BzK galaxies (sBzKs) in the proposed area. Therefore, it is expected that a few hundred dusty and massive high-redshift objects, which can be bright submillimeter sources, are detected from the proposed data.

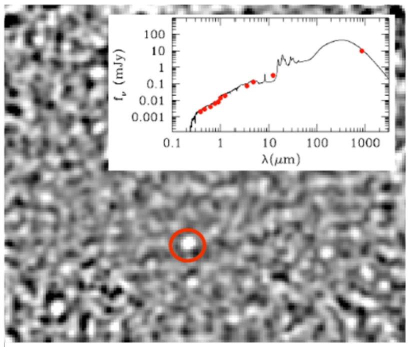

Figure 5 The example SCUBA-2 850μm image with RMS of 1.5mJy. The inset shows SED of the brightest source in the area. The SED fit was performed by using 850μm data and other survey data (CFHTLS, Infrared Medium-deep Survey and WISE). This object can be selected as both ERO and DRG.

The multi-wavelength data from optical to MIR we have are deep enough to detect objects having SEDs similar to the example shown in Fig. 5. This makes it possible to investigate detailed properties of various components through SED fitting and to compare those of different populations at various epochs. Additionally, the significant number of objects for each population in the proposed area allows us to perform stacking analysis to understand the average properties for faint objects statistically (e.g., Knudsen et al. 2005; Decarli et al. 2014). This unique dataset will provide an opportunity to link dusty galaxies at different cosmic epochs and to understand the evolution of galaxies.

2-2 Star formation and dust processing

While the mid-infrared PAH emission that is associated with the photo-dissociation regions in galaxies is one of the widely used star formation indicators, the far-infrared luminosity is regarded as a more robust probe of star formation since most of the energy from young stars is absorbed and re-emitted at FIR wavelengths. A correlation between different infrared star formation indicators, i.e., the PAH and FIR luminosity, is expected but may not be ubiquitous, especially for galaxies with undergoing violent activity (e.g., AGN, nuclear starburst, major merger). This is because the PAH particles are potentially destroyed by the strong UV radiation. In the local universe, ULIRGs and AGN-dominated galaxies show a deficiency in PAH emission. However at $z > 1$, it is reported that galaxies with IR luminosity similar to that of local ULIRGs still show strong MIR emission (e.g., Takagi et al. 2010). This means that physical conditions of the interstellar medium in star-forming galaxies for a given IR luminosity are different as a function of redshift. The dominance of PAH emission would result in different dust attenuation properties for galaxies at different redshifts. Since the study of high-redshift star-forming galaxies generally selected based on their intense star formation and strong UV (e.g., Lyman break galaxies; Steidel et al. 1999; Bouwens et al. 2009) always suffers from the uncertainties in dust attenuation measurements, the estimation of the dust attenuation in active star-forming galaxies at z > 1 would shed light on the construction of cosmic star formation history. Not only for high-redshift galaxies, the variation in PAH-to-FIR ratios among local star-forming galaxies would be a strong reference for understanding different physical parameters related in determination of ISM status.

One way to investigate the PAH-to-FIR ratio for local star-forming galaxies is to use the ratio between total IR luminosity and rest-frame 8μm luminosity ($IR8=L_{IR}/L(8\mu m)$) (Takagi et al. 2010; Murata et al. 2014). With the complete mid-infrared coverage over the NEP region, we can estimate rest-frame 8μm luminosity from z ~ 0 to z ~ 2 accurately (e.g., Kim et al. 2015). In order to derive FIR luminosity at these wavelengths, 850μm data is strongly required. Combining SCUBA-2 850μm data with the existing MIR data, can refine the PAH diagnostics that reflects the dust attenuation curve for high-redshift star-forming galaxies.

3. Co-evolution of SMBH and their Host Galaxies

One of the challenges of current large-area deep multi-wavelength surveys is the identification and reliable decomposition of different emission components that are usually superimposed in galaxies. In particular, the challenges of separating the emission coming from the accretion of matter onto a supermassive black hole (SMBH) and that of its host galaxy have been studied extensively in the literature (e.g., Feltre et al. 2012, Rocca-Volmerange et al. 2013, Leipski et al. 2014, Karouzos et al. 2014). The problem becomes more accentuated in the high-redshift regime, where resolution and sensitivity limitations come into play.

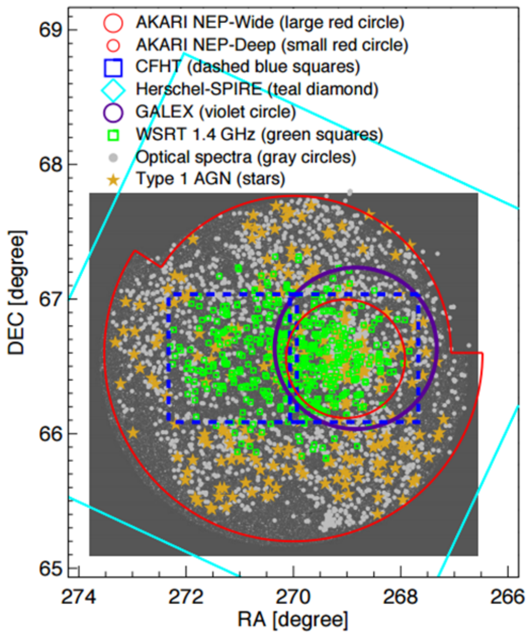

Figure 6. AKARI NEP-Wide multi-wavelength coverage. Green squares denote radio-detected sources at 1.4 GHz with WSRT. Yellow stars denote spectroscopically confirmed Type 1 AGNs, while all sources with optical spectra are shown with gray circles.

However, the importance of this separation cannot be overstated, as it relates to several of the most pressing questions at the frontiers of current astrophysical research on the formation and evolution of galaxies. While it is currently accepted that the peak of both the star formation and SMBH accretion activity in galaxies occurred sometime between 2-3 Gyr after the Big Bang (e.g., Richards et al. 2006, Hopkins & Beacom 2006), the potential dilution of either of these components from the other one is of yet not fully understood. Furthermore, there exists a set of scaling relations (e.g., Ferrarese & Merritt 2000, Gebhardt et al. 2000, Woo et al. 2013) that seems to link these two components. This implies a putative regulating mechanism exists that operates from one (or both) components to the other one (often coined as active galactic nuclei, AGN, feedback, e.g., Fabian 2012) that should bring about some degree of co-evolution between AGN and their hosts (e.g., Heckman & Best 2014). An accurate separation of the AGN from its host galaxy emission is imperative if any manifestation of AGN feedback is to be discovered.

The NEP survey field and its multi-wavelength dataset is uniquely equipped to face the challenge of both identifying galaxies that harbour an actively accreting SMBH and reliably decomposing its emission from that of its host galaxy. There are at least four ways that we can currently employ to identify AGN in the AKARI-NEP field: (1) mid-IR emission (e.g., Takagi et al. 2007, Hanami et al. 2012), (2) radio emission (e.g., Karouzos et al. 2014), (3) optical spectroscopy (Shim et al. 2013, Takagi et al., in prep.), and (4) X-ray emission (Krumpe et al. 2015) that however is confined in the Deep part of the survey. A coverage map, similar to Fig. 1, showing the radio and optical spectroscopic observed sources in the NEP, together with the Herschel, GALEX, and CFHT coverage of the field is shown in Fig. 6. Beyond the actual AGN identification, the contiguous coverage in the near- to mid-IR wavelengths from AKARI and the extensive ancillary datasets provide a unique tool for the precise estimation of both the AGN power (bolometric luminosity, accretion power, jet power, etc.) and the degree of ongoing star formation in these galaxies (stellar mass, star formation rate, stellar ages, metallicity, etc.). We are thus in a unique position to attack the questions discussed above.

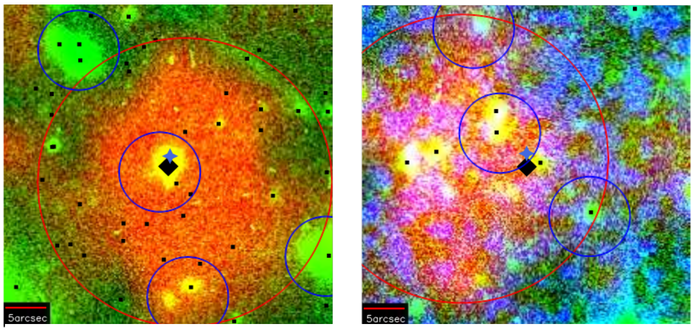

Figure 7. Two examples of cross-matching between an IR-radio cross-matched source, a GALEX sources, and a Herschel source. Images are RGB composites of the Herschel-Spire 250μm band (R), the CFHT r-band (G), and the GALEX NUV band (B). The blue star denotes the position of the radio sources, the black diamond shows the position of the cross-matched AKARI source, and black squares note the position of other detected optical sources. Blue circles mark the position and beam size of GALEX, while red circles denote Herschel-SPIRE sources. In both cases the Herschel-SPIRE beam contains several GALEX sources (UV-bright sources are expected to be star-forming galaxies that would thus also contribute significantly to the aperture-integrated far-IR measured by Herschel-SPIRE.

A JCMT SCUBA-2 850μm survey of the full NEP area will fill an obvious gap in our broad band emission characterization of these AGN, situated between the reddest Herschel-SPIRE channel at 500μm and our WSRT radio data at 1.4 GHz. As mentioned above, 850 μm flux information will be crucial in constraining the tail of the far-IR hump coming from the cold (~10 K) dust re-radiated emission of young (<100 Myr) stellar populations, hence allowing a far more robust estimation of ongoing star formation, as well as cold dust masses and temperatures (e.g., Casey et al. 2013). Potentially even more importantly, the 850 μm measurements with SCUBA-2 will allow a far better localization and cross-identification of the far-IR emission from Herschel with emission at shorter wavelengths. The resolution issue of Herschel SPIRE and in a lesser degree PACS data is clearly shown in Fig. 7, where RGB images of examples of radio-AGN are shown that potentially suffer from confusion in the far-IR due to the large beam size of Herschel (FWHM~35 arcsec at 500μm). The confusion issue has been very clearly illustrated in the case of low-resolution sub-mm observations of SMGs (e.g., Hodge et al. 2013, Barger et al. 2014).

In the following we briefly describe 3 particular scientific themes that will be addressed with the combination of already available data and the newly-acquired SCUBA-2 data.

3-1 The impact of radio jets on star formation in their hosts

In Karouzos et al. (2014) we explored the star formation properties of radio-selected AGN in the AKARI-NEP field (both Wide and Deep) by decomposing their broadband SEDs. The far-IR hump was constrained by the Herschel-SPIRE measurements. Of a total of 321 1.4GHz radio-detected sources with AKARI counter-parts, 68 sources are detected by Herschel-SPIRE. This fraction is expected to be larger for the Herschel-PACS detections (data reduction is currently ongoing). We found tentative evidence that the star-formation per unit stellar mass appears to decrease as a function of radio jet power.

Using the SCUBA-2 850 μm flux measurements and an increased radio-selected sample, based on both the 1.4 and 0.6 GHz radio data, we will improve upon our SED modeling by: (i) constraining the drop-off of the cold-dust emission spectrum, (ii) making a more robust cross-matching between far-IR and mid-IR/optical counterparts, and (iii) including physically motivated modeling of the stellar component of these sources (using the CIGALE code developed by some of the co-Is of this proposal, e.g., Buat et al. 2014, Ciesla et al. 2014). We will complement our individual source fitting by a stacking analysis in the far-IR to sub-mm (Herschel + JCMT) of the radio-sources not individually detected (e.g., Kalfountzou et al. 2014). Deliverables of the SED modeling include star-formation rates, stellar ages, cold dust masses and temperatures, as well as AGN radio and bolometric luminosities. We will use this information to further explore the potential impact of radio jets on their host ISM star formation properties.

3-2 Searching for hidden, dust-obscured AGNs and their contribution in star formation

We will model the SEDs of these AGN and derive the AGN-decomposed far-IR luminosity and AGN bolometric luminosity, using the superior far-IR/sub-mm coverage offered by the combination of Herschel and JCMT. We also utilize the new X-ray data to classify the AGN candidates. eROSITA (expected to be launched in early 2018) will conduct all-sky survey over four years; but due to the design nature of the spacecraft, NEP is the highest visibility region. Fig. 8 shows the X-ray spectra of obscured (Compton thick (CT), $N_H > 10^{24}$ cm^{-2}, where N_H is hydrogen column density) and unobscured (Compton thin) AGN (Ueda et al. 2014), and eROSITA energy range is critically important to discriminate them. As for the optical part of the SED, we recently took deep Subaru HSC data over the AKARI NEP-Wide image, and a few-million band-merged source catalogue is almost ready to select the AGN candidates by the SED fitting.

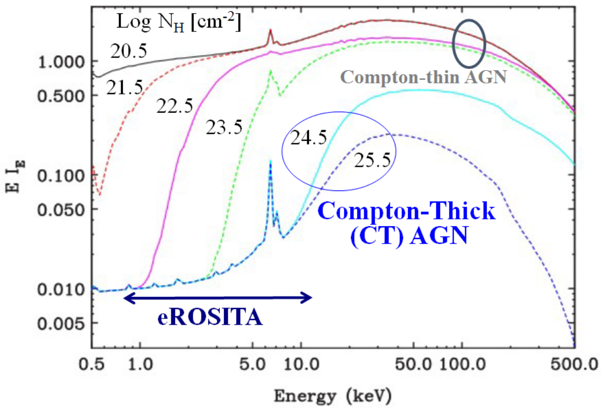

Figure 8. Rest frame X-ray spectra of various absorption levels with same intrinsic power (Ueda et al. 2014). X-ray photons going through a hydrogen column of N_H~10^{24} cm^{-2} gas is subject to Compton scattering.

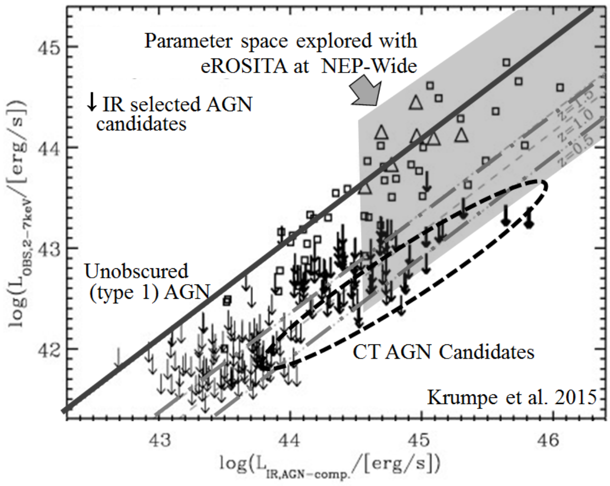

Figure 9. $L_{IR,AGN\text{-}comp}$. (IR Luminosity of the AGN component derived from the SED fitting) vs $L_{OBS,2\text{-}7\,keV}$ (observed 2-7 keV luminosity of X-ray sources detected with Chandra in NEP-Deep (Krumpe et al. 2015). Redshift-dependent dash-dotted lines corresponding to log N_H ~24, below which the object is a strong Comptonthick AGN candidate. 28 strong Compton-thick candidates are indicated by a broken circle. Grey area indicates parameter space to be probed by the 5.4 deg2 AKARI & eROSITA NEP-Wide data. Note that $L_{OBS,2\text{-}7keV}/L_{IR,AGN}$ is an indicator of absorption.

In Fig. 9, IR Luminosity of the AGN component (derived by the SED fit) vs X-ray luminosity for sources detected with Chandra is shown. Although sky coverage is limited to 0.25 deg^2 we found ~30 CT AGN candidates based on existing Chandra X-ray data (Krumpe et al. 2015). Although sky coverage is limited to 0.25 deg^2 we found ~30 CT AGN candidates based on existing Chandra X-ray data (Krumpe et al. 2015). With e-ROSITA data covering the entire NEP-Wide field, ~300 semi CT AGNs ($N_H \geq 10^{23.5}$ cm^{-2}) in $0.4 < z < 2.4$ will be discovered, together with similar number of Compton-thin AGNs at hard X-ray (2-10 keV) and ~3000 AGNs in the soft X-ray (0.5-2 keV), based on the expected 5 σ flux limit of 2.9×10^{-14} erg s^{-1} cm^{-2} (2-10 keV) and 2.0×10^{-15} erg s^{-1} cm^{-2} (0.5-2 keV) for the expected exposure time (~35 ks) over the deepest e-ROSITA region including entire NEP-Wide area.

4-3-3 A census of AGN broadband emission

Finally, given the superior coverage of the mid- to far-IR wavelengths (by the combination of AKARI, Herschel, and JCMT), we will use our samples of differently selected AGN (spectroscopic, radio, mid-IR, etc.) to produce much better sampled composite SEDs of each AGN type than previous studies (e.g., Hatziminaoglou et al. 2010, Kalfountzou et al. 2014) and will more precisely constrain the intrinsic AGN contribution in the far-IR (e.g., Mullaney et al. 2011). For example, out of 237 radio sources at 1.4 GHz, 82 can be classified as radio AGN. We also tentatively identified 1755 AGN candidates based on their colors in AKARI bands. Due to the unique and homogeneous coverage of the mid-IR by the AKARI IRC, in particular the bands around 9 and 11 μm that cover the PAH and silicate features of star-forming regions and AGN, respectively, and which Spitzer notably lacked, the construction of such composite SEDs is of legacy value for similar future studies that will be enabled by instruments such as the JWST and SPICA for order of magnitude larger and deeper samples. The much better wavelegnth sampling of these composite SEDs will further allow us to model them and gain insight of the statistical properties of the different AGN populations probed at different wavelengths.